COMSOL CONFERENCE 2020 NORTH AMERICA

Conductance Modeling of Flexible Organic Thin Films for Solar Cell Devices

C. Carradero Santiago[1], J. Vedrine-Pauléus[2]
1. Materials Science and Engineering, Youngstown State University, Youngstown, OH, USA
2. Department of Physics & Electronics, University of Puerto Rico at Humacao, Humacao, PR, USA

Corresponding author
Email: Carolyn.Carradero@upr.edu

Abstract

In this research work, we developed a virtual model to examine the electrical conductivity of multilayered thin films when positioned above a single layer and multilayers of graphene, and flexible polyethylene terephthalate (PET) substrate. Additional structured thin films were configured as follows: organic layers of poly(3,4-ethylenedioxythiophene) polystyrene sulfonate (PEDOT:PSS) as a hole conducting layer, poly(3-hexylthiophene-2,5-diyl) (P3HT), as p-type, phenyl-C61-butyric acid methyl ester (PCBM) as n-type photoactive layers, and aluminum (Al) added as the top conductor. COMSOL Multiphysics was the primary simulation tool used to develop the virtual model that enabled us to analyze the variations in electric potential and conductivity throughout the thin-film structural system. Using the AC/DC Electromagnetic application, electric currents module we defined the geometry of each layer and input properties for an organic photovoltaic (OPV) configuration.

Keywords: organic thin-films, graphene, solar cells

1.0 Introduction

Organic photovoltaic (OPV) solar cells or plastic solar cells have attracted attention because they can be deposited on flexible, lightweight substrates using low cost and simpler fabrication methods. An essential aspect of these thin films is the transparency and conductivity of the electrode through which light transmit in and out of the device. OPV devices can enable the fabrication of large area solar cells on printable and flexible substrates, but increasing their efficiency is coupled to understanding the functional chemistry, and nanoscale engineered properties. Currently, organic based solar cells have a low sunlight to electricity conversion. Increasing their efficiency is complex based on the inherent characteristic of these donor and acceptor polymers. Although they can be synthesized and tuned to receive more coverage of the solar spectrum than conventional inorganic PVs, their highly amorphous structure, and strong exciton interaction through the amorphous polymer leads to decrease electron transfer and low power-conversion efficiencies (PCE). The potential route of using graphene layers or graphene oxide as a transparent electrode in place of indium tin oxide (ITO) provides advantages to flexible solar cell devices that could be relevant to aerospace technologies, wearable and flexible optoelectronic devices (Yin et al., 2010; Park et al., 2012).

The ease of processing flexible OPVs including doctor blade, and spin-coating processes, roll-to-roll, ink-jet printing presents an attractive alternative to more complex and expensive ITO deposition processes. Indium tin oxide (ITO) is broadly used in solar cell, and electronic display and device applications, but for flexible device solar cells (Girtan and Rusu, 2010), ITO is considered too expensive and limiting for being brittle which will restrict its use on flexible substrates (Alzoubi et al., 2011). For this reason graphene has been researched as a substitute for ITO for flexible electronics. Graphene is a monolayer of carbon atoms, tightly packed in a two-dimensional hexagonal honeycomb lattice (Geim and Novoselov, 2007). It has a structure of a plane of sp^2-bonded atoms with a molecule length of 0.142 nanometers. Layers of graphene stacked on top of each other form graphite with interplanar spacing of 0.335 nanometers. Graphene has highly translucent, with an optical transmittance greater than 90%, and high electrical conductivity, in addition to high chemical and thermal stabilities (Nair et al. 2008). The implications of replacing ITO with graphene provide a challenging route for making highly flexible, durable. ITO is a very good and ubiquitous transparent conductor, currently used in optoelectronic devices, but ITO cracks under stress making it suboptimal as a ceramic for flexible electronic applications. Possible replacement using carbon nanotubes has also been researched for flexible electronics, but there are some challenges on the uniformity and commercial applications using this method. The coating of monolayers or well-deposited multilayers of graphene is at an infancy stage, but the potential for use in flexible electronic devices has numerous rewards.

Polyethylene terephthalate (PET) has flexible bendable and mechanically stable properties and is highly transparent. PET has been extensively researched as a viable substrate in electronic displays (Gorkhali et al., 2002; Vedrine 2005), thin-film-transistors applications, wearable technologies, and as a substrate for deposition of carbon nanotube paints, (Pang et al., 2013). While chemical vapor deposition (CVD) is well researched for fabricating graphene (Egberts et al., 2014; Oquendo et al., 2014), the transfer of graphene sheets from the deposited substrate onto PET poses various challenges because of defects that are introduced from

the transferring techniques. Some researchers have been successful in fabricating graphene from CVD, and have transferred graphene sheets from Cu foil to PET substrates with minimal contamination (Sinitskii Group), including, for example inkjet printing of graphene (Gao et al., 2014).

Generally, graphene based OPVs do not yield better performance when compared to ITO-based devices. For a four-layer electrode of graphene, the absorption loss is the main performance-limiting factor, even when it has similar transmittance to ITO on a glass electrode (Koh et al., 2014). Another limiting factor of graphene compared to ITO is that the power conversion efficiency is less than 50%. The work by Yusoff and coworkers presents the incorporation of graphene in semi-transparent OPVs to achieve a 45% transmission but with 8.02% efficiency (Yusoff et al. 2014). In comparison to ITO, graphene performs better with small molecules like ZnPc:C_{60} device than with the P3HT:PCBM when compared to their respective optimized ITO-based device. The tandem device structure have been shown to have higher conversion efficiencies with slightly greater than 17%, in OPVs (Chen et al., 2018).

2.0 Methods

In this work, we used a planar donor-acceptor heterojunction configuration instead of the bulk-heterojunction (BHJ) device structure that tends to dissociate exciton more efficiently at the donor-acceptor interfaces. The majority of OPV devices is integrated monolithically, and uses stripes of different layered materials in a stack configuration. For this simulation, a simplified structure was designed to reflect a single striped stack, with the connection made between top (Al) and bottom electrodes (graphene) electrodes.

Simulations were completed in COMSOL version 5.2 (Build 220), COMSOL Multiphysics and the AC/DC modules were used. All units are in International System Units (SI). For each model, a coordinate system with names and boundaries was defined.

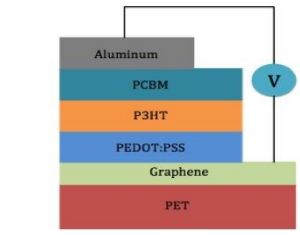

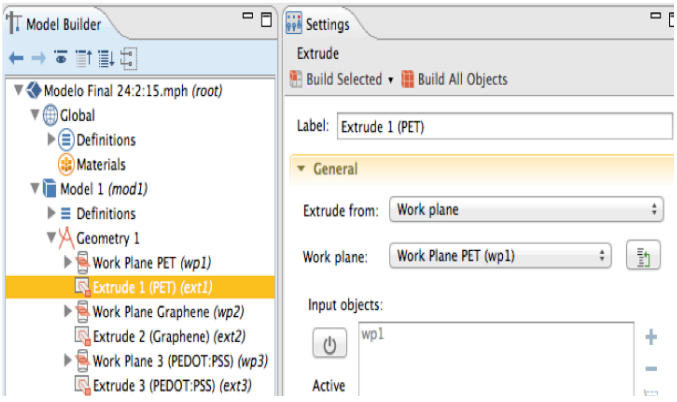

	Property	Name	Value	Unit
✓	Electrical conductivity	sigma	960*10e-6[S/m]	S/m
✓	Relative permittivity	epsilonr	1	1
	Relative permeability	mur	1	1
	Heat capacity at constant pressure	Cp	2100[J/(kg*K)]	J/(kg·K)
	Surface emissivity	epsilon_rad	1	1
	Density	rho	0.0077[kg/m^3]	kg/m³
	Thermal conductivity	k	4000[W/(m*K)]	W/(m·K)
	Resistivity	res	10e-6[Ω*m]	Ω·m
	Young's modulus	E	0.5	Pa

Property	Name	Value	Unit
Coefficient of thermal expansion	alpha	150e-6[1/K]	1/K
Heat capacity at constant pressure	Cp	1900[J/(kg*K)]	J/(kg·K)
Relative permittivity	epsilonr	2.3	1
Density	rho	930[kg/m^3]	kg/m³
Thermal conductivity	k	0.38[W/(m*K)]	W/(m·K)
Electrical conductivity	sigma	10e-21	S/m
Young's modulus	E	1e9[Pa]	Pa
Poisson's ratio	nu	1	1

Figure 1. Image of general solar cell layered configuration, and material property values for each monolayer (top); depicts the model builder COMSOL Multiphysics, and positioning and geometry of each layer and work plane (middle); material properties table for each layer and - PET and of graphene are shown (bottom) .

Figure 1 displays the general structure of the solar cell constructed in the simulation, with poly(3,4-ethylenedioxythiophene) polystyrene sulfonate (PEDOT:PSS) as a hole conducting layer, poly(3-hexylthiophene-2,5-diyl) (P3HT), as p-type, phenyl-C61-butyric acid methyl ester (PCBM) and aluminum top transparent conductor. For each layer, the spatial positioning, and work planes were added followed by the material properties for all layers, to closely corroborate with experimental work. The properties of PET and of graphene are shown here.

The geometry for each model included special dimensions, x,y,z coordinates, (length, width, height) specified in nanometer (nm), and angular units in degrees. The model geometry description was then defined for all given boundaries, edges, and vertices. Each layer in the design was given a plane geometry, or work plane to generate a reference or spatial positioning. The first layer in our design was the polyethylene (PET) work plane with a thickness of 50 nm, followed by graphene, with the defined dimensions for three layers of graphene at 1.02 nm thick, a layer of PEDOT:PSS with 80 nm thickness, P3HT with 60 nm, a 60 nm of a PCBM layer, and a 60 nm layer of aluminum. Since the thickness of the PET is much greater than that of graphene and successive thin films, we minimized the PET layer in the study to enable comparative planes between layers. Initially, we defined the 3D geometry of the model; in this case we want to incorporate six layers, so we generated six cubic squares, one on top of another. We then added the materials and assign PET as the lowest layer followed by graphene, PEDOT:PSS, P3HT, and PCBM as midsection layers, and aluminum as the top conducting layer. Since we wanted to analyze the electrical conductivity, we introduced the electric current equations. The material properties for each layer were specified and assigned. Properties such as relative permittivity, electrical conductivity, coefficient of thermal expansion, thermal conductivity, heat capacity; and mechanical properties including the Young's modulus, Poisson's ratio were recorded for each material, within the selected domain.

The Electric Currents used the COMSOL Multiphysics and AC/DC modules, with these governing equations:

$$\nabla \cdot J = Q_i \quad (1)$$
$$J = \sigma E + J_e \quad (2)$$
$$E = -\nabla V \quad (3)$$

(1) The continuity equation for local charge conservation derived from Maxwell's equation; (2) Ohm's Law with current density, conductivity and displacement current factor; where σ approaches infinity for perfect conductors, and 0 for insulators; and (3) The electric potential-electric field **E** as the gradient of the scalar potential *V*. Electrical insulations were placed around the cell to isolate the boundary conditions in order for COMSOL to function properly, and defined as follows:

$n \cdot J = 0$ (electric isolation)
$-n \cdot J_n = 0$ (inward current density)
$n \cdot (J_1 - J_2) = Q_i$ (boundary current source)

When the electric insulation was inserted, the equations above were used to formulate the proper isolation; a ground terminal was allocated, and current source at the boundaries was assigned.

3.0 Results and Discussion

Figure 3 depicts a detailed view of the layers in the software, the Terminal 1 bias of 5V, the Terminal 2 bias of -5V as well as the meshing necessary to solve the equations. We also apply bias voltages of +5V and -5V between conducting layers of graphene and aluminum, respectively, to determine the resulting electric variation across the layers.

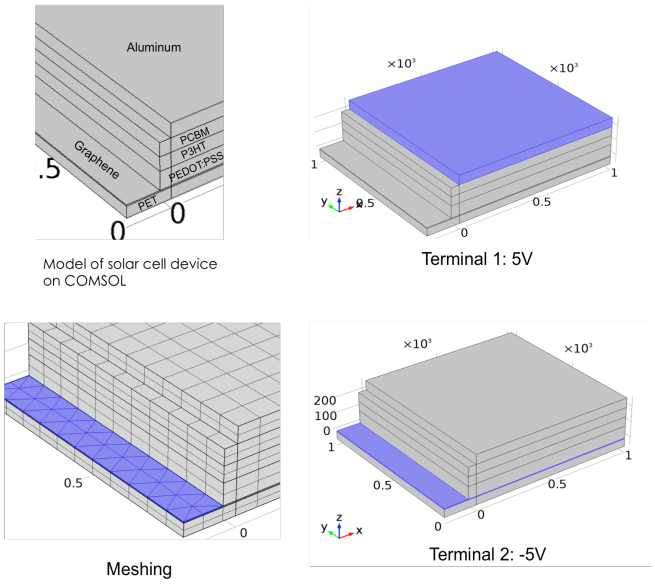

Figure 3. Constructed models of solar cell device structured thin films configuration: PET/graphene/PEDOT:PSS/P3HT:PCBM/Al; Meshed analysis of structures; assigned top (Al) and bottom (graphene) layers as terminals 1 and 2, respectively with voltage biases applied at terminals highlighted.

As a result, we obtained a 3D simulation model that demonstrates the behavior of the surface electric potential across the thin film layers with an applied bias at the terminals, as shown in Figure 4, for a -5V to +5V voltage bias sweep. Note that the results presented show PET positioned at the negative z-axis (-50 nm), with the graphene layer starting at 0 nm; thus the results shown for voltage and current activated at the graphene layer, or at the positive z-axis. The scale bar indicator demonstrates the relative electric potential at each layer, as shown from dark blue, of -5 V applied at the graphene layer transitioning to dark red at +5 V.

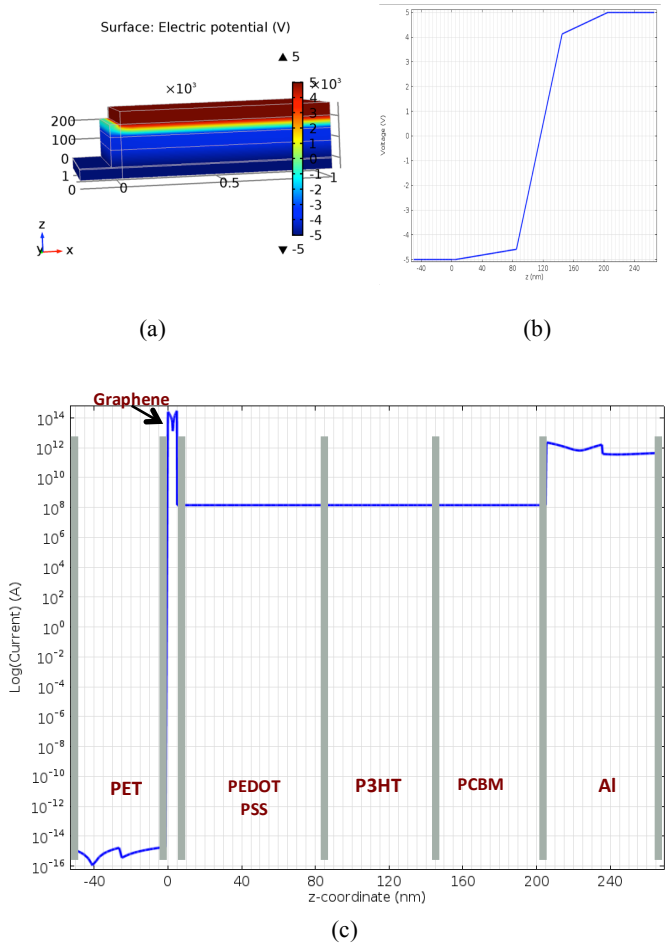

Figure 4. The electric potential difference across each section of thin film layers is depicted (a); voltage potential across the z-axis (b); the logarithm of current vs. position along z-axis through the multilayered structure (c).

The resulting simulation of current through the multilayered structure shown in Figure 4 (c) depicts the resulting current behavior at the graphene layer to be extremely high, then stabilizes with magnitude lower for the subsequent organic conductors PEDOT:PSS, P3HT, and PCBM, followed by a slight rise in conductance at the aluminum surface. The sharp transition in conduction at the three layers of ideal graphene is indicative of its high electric mobility, and high electrical conductivity, in the ease of electron transition through the simulated few layered structure for the defined material properties.

4.0 Conclusions

We analyzed the electrical conductivity across multilayers of thin films to simulate electric potential in an organic solar cell with graphene as the transparent conductor situated on a flexible PET substrate. In the Multiphysics and AC/DC suites, electric current equations are added to analyze response and behavior of the electric potential across the multilayered thin film materials. As a result, we obtained a 3D simulated model that shows the behavior of the electric potential across the thin film layers from PET to Al with electrical conductivities of 10^{-21} and 35.5^{+6} [S/m], respectively. The electric potential between the organic polymer layers alone shows a gradient in color indicating variation in current as a result of their distinct material properties, and reaction to a bias applied. Future work would include fine-tuning this simulation, and assess variation in electric conductance with graphene to graphite layers, and with the use of the bulk heterojunction active layer configuration. This simulation allowed us to analyze the electrical conductivities, and visualize the model with varying voltage potential, and bias across the conducting substrates, to better visualize potential experimental configurations, valuable in fabricating organic thin films in solar device applications.

References

1. Yin, Z., Sun S., Salim T., Wu S., Huang X., He Q., Lam Y.M., and Zhang H. Organic Photovoltaic Devices Using Highly Flexible Reduced Graphene Oxide Films as Transparent Electrodes. ACS Nano, 4, 9, 5263–5268, (2010).
2. Park, H., Brown, P. R., Bulović, V. and Kong, J. Graphene as transparent conducting electrodes in organic photovoltaics: studies in graphene morphology, hole transporting layers, and counter electrodes. Nano Lett. 12, 133–140, (2012).
3. Girtan, M., and M. Rusu. Role of ITO and PEDOT:PSS in Stability/degradation of Polymer:fullerene Bulk Heterojunctions Solar Cells. Solar Energy Materials & Solar Cells 94 (3): 446–50, (2010).
4. Alzoubi, K., Hamasha, M. M., Lu, S. and Sammakia, B. Bending Fatigue Study of Sputtered ITO on Flexible Substrate. Journal of Display Technology, vol. 7, no. 11, 593-600, (2011).
5. Geim, A. K., and K. S. Novoselov. "The Rise of Graphene." Nature Materials 6 (3): 183–91 (2007).
6. Nair, R. R., P. Blake, A. N. Grigorenko, K. S. Novoselov, T. J. Booth, T. Stauber, N. M. R. Peres, and A. K. Geim. Fine Structure Constant Defines Visual Transparency of Graphene. Science 320 (5881): 1308, (2008).
7. Gorkhali, S. P., Cairns, D. R., Esmailzadeh, S., Vedrine J., and Crawford, G. P. A Comparison of the Thermo-Mechanical Reliability of Organic and Inorganic Transparent Conducting Electrodes for Flexible Displays. Society for Information Display - Proceedings of Asia Display 7, 331-334, (2002).
8. Vedrine, J. A., Electromechanical analysis of transparent conducting substrates for flexible display applications [Doctoral dissertation, Brown University]. ProQuest Dissertations Publishing, (2005). 3174688.
9. Pang, C., Lee, C, Suh, K. Y. Recent Advances in Flexible Sensors for Wearable and Implantable Devices. J. Appl. Polym. Sci. (2013).
10. Egberts, P., Han, G. H., Liu, X. Z., Johnson. A. T. C., and Carpick, R.W. Frictional Behavior of Atomically Thin Sheets: Hexagonal-Shaped Graphene Islands Grown on Copper by Chemical Vapor Deposition. ACS Nano, Vol. 8, NO. 5, 5010–5021, (2014).
11. Oquendo, M., Calderon, G., Vedrine-Pauléus, J., Hee, G. and A.T. Johnson Jr., Pinto, N. Charge transport in CVD graphene. Proceedings of The National Conference On Undergraduate Research (NCUR), 820-825, (2014).
12. Gao, Y., Shi, W., Wang, W., Leng, Y. and Zhao Y. Inkjet Printing Patterns of Highly Conductive Pristine Graphene on Flexible Substrates. Ind. Eng. Chem. Res., 53, 16777−16784, (2014).
13. Koh, W.S., Gan, C.H., Akimov, Y., Bai, P. The Potential of Graphene as an ITO Replacement in Organic Solar Cells: An Optical Perspective, IEEE Journal of Selected Topics in Quantum Electronics, (2014).
14. Yusoff, A. R., Lee, S.J, Shneider, F., da Silva, W. Jang, J., High-performance semitransparent tandem solar cell of 8.02% conversion efficiency with solution-processed graphene mesh and laminated Ag nanowire top electrodes. Adv. Energy Mater. 4, 1301989, (2014).
15. Chen, Y.; Cao, Y.; Yip, H-L.; Xia, R.; Ding, L.; Xiao, Z.; Ke, X.; Wang, Y.; Zhang, X. Organic and solution-processed tandem solar cells with 17.3% efficiency. Science 361 (6407): 1094–1098, (2018).
16. Lang, U., Naujoks, N. and Dual, J. Mechanical characterization of PEDOT:PSS thin films. Synth. Met. 159, 473–479, (2009).
17. Liu, J., Wang, X., Li, D., Coates, N.E., Segalman, R.A., Cahill, D.G. Thermal Conductivity and Elastic Constants of PEDOT:PSS with High Electrical Conductivity. Macromolecules 48, 585–591, (2015).
18. Lilliu, S, Agostinelli, T, Pires E, Hampton M, Nelson J. and Macdonald J. Dynamics of Crystallization and Disorder during Annealing of P3HT/PCBM Bulk Heterojunctions. Macromolecules 44, 2725–2734, (2011).
19. Duda, J. C., Hopkins, P. E., Shen, Y. and Gupta, M. C. Thermal transport in organic semiconducting polymers. *Appl. Phys. Lett.* 102, 251912, (2013).
20. Ngo, T. T., Nguyen, D. N. and Nguyen, V. T. Glass transition of PCBM, P3HT and their blends in quenched state. *Adv. Nat. Sci: Nanosci. Nanotechnol.* 3, 045001, (2012).

Acknowledgements

This work funded by the NASA-IDEAS Grant NNX10AM80H and NNX13AB22A, and by NSF-DMR-1523463 (PREM), and NASA Grant No. 80NSSC19M0049; Thankful for discussions with Dr. Alexander Sinitskii at UNL.